HIFE-Haptic Interface for Finger Exercise

Uroš Mali and Marko Munih, *Member, IEEE*

***Abstract*—A haptic device with two active degrees of freedom and a tendon-driven transmission system was designed, built, and tested. It was constructed as a mechanism with a small workspace that envelops a finger workspace and can generate forces up to 10 N, suitable for finger exercise. Kinematic and dynamic model equations of the haptic device are presented in the paper. The control strategies, the implementation of the application on a PC, the real-time millisecond-class control environment, running under the MS Widows operating system, and safety mechanisms are described. Also, the duration test for the maximum sustained output force, and validations of accuracy of the output force and the consistency of the followed path, were performed. The performance, accuracy, and safety of the device were found to be very good, which makes the device suitable for rehabilitation purposes.**

***Index Terms*—Control, dynamic equations, dynamics, haptic device, kinematics, real time, rehabilitation.**

I. Introduction

HAND and finger injuries are one of the leading causes of activity limitation in everyday life [1], [2]. The rehabilitation process after injury or finger paralysis can be lengthy. Usually, treatment takes place at a clinic where an occupational therapist advises exercises according to a treatment program. Through the rehabilitation process, the therapist applies certain forces to the injured finger to regain its strength and range of motion. Therefore, an interface that could imitate the therapist's exercises would be beneficial. The interface should have possibilities of position and force control. Haptic devices, which can, by definition, generate controlled force to a single finger, were selected as a suitable type of device for the application of exercising the finger.

Active haptic interfaces provide the opportunity to enhance the interaction beyond what is normally possible with passive mechanical controls, such as a computer mouse or joystick. They can be used both to display and control forces, and adjust their behavior to reflect or transmit context changes [3], [4]. Today, there are many devices that use haptic technology and are commercially available. For example, force feedback joysticks and similar devices were among the earliest developed for the mass market in the mid-1990s. Later, more sophisticated mechanisms were developed [5], and some of them could be appropriate for the proposed finger application [6]–[10].

The most widely used haptic devices at present are the PHANToM family of backdrivable robotic arm manipulators [6], [8] by SensAble Technologies. In spite of very good construction and variety of the models, its main drawbacks are low sustained resistive force of only up to 3 N, and high cost. CyberGrasp [9] is another innovative force-feedback system for the fingers and hand. It is a force-reflecting exoskeleton that fits over a CyberGlove, which adds finger position sensing. The advantage is that it provides resistive force feedback to each finger. The disadvantages are only one degree of freedom (DOF), that only extension resistive force feedback is applied, and that it becomes difficult to bear after a few minutes if not sustained by the CyberForce armature. Furthermore, the Rutgers Master II newly designed force-feedback glove [10] is a haptic interface for dexterous interaction with virtual environments, and is a follow-up to an earlier Rutgers Master II haptic interface [11]. It can provide a force feedback of up to 16 N to the thumb, index, middle, and ring fingertips. The high value of the applied force is an advantage over similar haptic devices, but a drawback is its design, where the placement of the actuators in the palm prevents the complete closing of the hand during grasping.

Despite such a variety of haptic devices, there is no device that adequately fulfills all the major demands for a finger exercise application. Either the continuous output forces are too low, or the workspace has limited size. The workspace should cover the entire human finger range of motion and requires continuous forces that lie most often in range of up to 10 N. Massie *et al.* [6] and Jones [12] pointed out that people rarely exert more than 10 N of force during precise manipulation. The HIFE meets both requirements with higher continuous output force and a properly sized workspace. An important factor is also the cost of the device, which should be as low as possible. The approximate cost of the present system is in range of €4000, with further reduction possible.

The mechanism of a haptic device shown here is lightweight and backdrivable, with two active DOFs and two passive DOFs at the point of finger attachment. It is actuated by two direct-current (dc) motors placed on the base of the device. Such haptic display design and configuration allows the estimation of finger forces acting at the attachment point without using force/torque sensors.

In-house design allowed the development of an accurate dynamic model of the haptic device. The unknown model parameters were identified to achieve model responses similar to the actual system. The model derived this way was used for estimating forces at the tip of the device, and for controlling the required motor torques. Separate torque contributions can be identified within the model; e.g., Coriolis and centripetal, gravity, etc.

To take full advantage of the proposed haptic interface setup, the real-time and software demands must also be met. Crucial are the location of the main functional elements within software modules, communication between the modules, and the ability to craft and customize low level details of the haptic control code. Various timing and other practical demands should be fulfilled when dealing with real-time control systems [13], [14].

Manuscript received April 10, 2004; revised July 9, 2004 and November 11, 2004. Recommended by Technical Editor C. Mavroidis.

The authors are with the Laboratory of Robotics and Biomedical Engineering, Faculty of Electrical Engineering, University of Ljubljana, SI-1000 Ljubljana, Slovenia (e-mail: urosmali@robo.fe.uni-lj.si; marko@robo.fe.uni-lj.si).

Digital Object Identifier 10.1109/TMECH.2005.863363

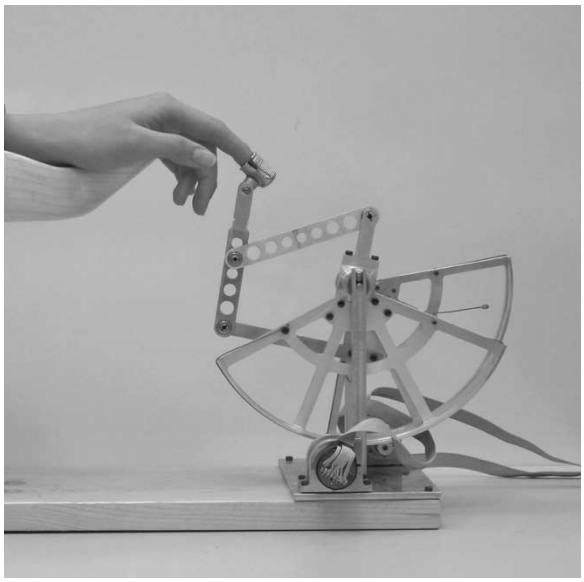

Fig. 1. Haptic device for finger exercise.

This paper presents a real-time control method which uses a parallel port interrupt line as an interconnection to an accurate external timing source.

The paper is organized into four main sections. First, the design requirements, where a workspace based on finger dimensions, grip forces, and issues of mechanical construction, are considered. The kinematics and dynamics of the device with force characteristics analysis are then described in Sections III and IV. Next is the control structure and accompanying electronics description, as well as an innovative solution for real-time control within the MS Windows environment. Also, the experimental data regarding the consistency of the followed path are presented in Section. The conclusions are given in Section VI.

II. Haptic Device Structure

A wide variety of haptic devices are now available. However, the one presented in this paper was designed especially for finger exercise. A haptic device should be capable of conveying realistic grounded forces to a human finger. The device's workspace should be large enough to cover or exceed the finger workspace. Furthermore, a compromise is needed between the haptic device workspace size and the available output forces. A haptic device that fulfills these requirements is presented in Fig. 1.

A. Mechanical Design

To obtain an appropriate workspace size, the human finger workspace range from known finger dimensions and range of motions was first calculated. The anthropometric data on fingers used for the finger workspace size calculation were taken from [15] and are presented in Table I. Mean values of phalanges lengths were used for calculation. Table II presents adequate finger joint extension and flexion angles according to Jones [12].

TABLE I
Phalange Lengths

Phalanges	Max / mm	Mean / mm
Proximal	54	47
Medial	36	30
Distal	30	25

TABLE II
Phalanges Joint Angles

Joint	Flexion	Extension	Notes
MCP	85°	-40°	Flexion rises from II. to V. finger for about 5°
PIP	100°	0°	Same for all fingers
DIP	80°	0°	Same for all fingers

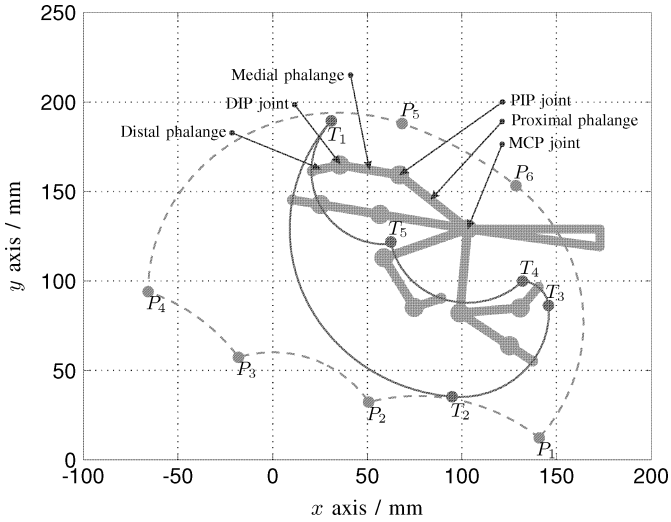

Fig. 2. Haptic device workspace range wrapped around the finger workspace.

From known finger segment lengths and the known range of motion for each segment, the finger workspace range boundaries were calculated as shown in Fig. 2 with a solid line. The boundary starts at point T_1 with the finger fully extended. From point T_1 to point T_2, the metacarpophalangeal (MCP) joint angle changes from full extension to full flexion. From point T_2 to point T_3, the proximal interphalangeal (PIP) joint angle changes from full extension to full flexion, and further on to point T_4, the distal interphalangeal (DIP) joint angle changes to full flexion. Between points T_4 and T_5, the PIP and DIP joint angles stay at full flexion, but the MCP joint goes to full extension. At the end the PIP and DIP, joint angles simultaneously vary from their maximum flexion to maximum extension at point T_1.

After considering a number of mechanisms that would cover such an envelope, the mechanical structure presented in Fig. 3 was selected. It is based on a very lightweight parallel mechanism where the end-effector (finger attachment) is connected to the base by two independent kinematic chains. Also, the workspace size was optimized with segment lengths according to the size of the finger workspace range. When selecting segment lengths (100 mm each), the workspace range of the

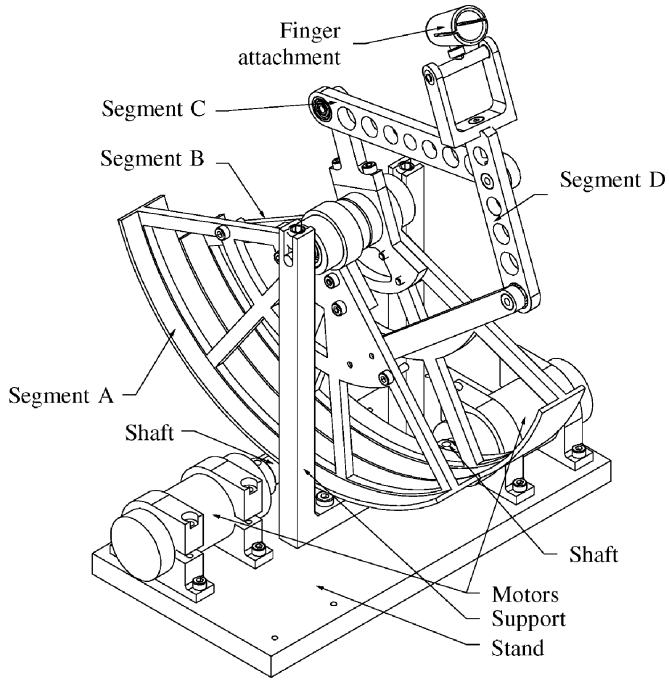

Fig. 3. Three-dimensional (3-D) model of the haptic device.

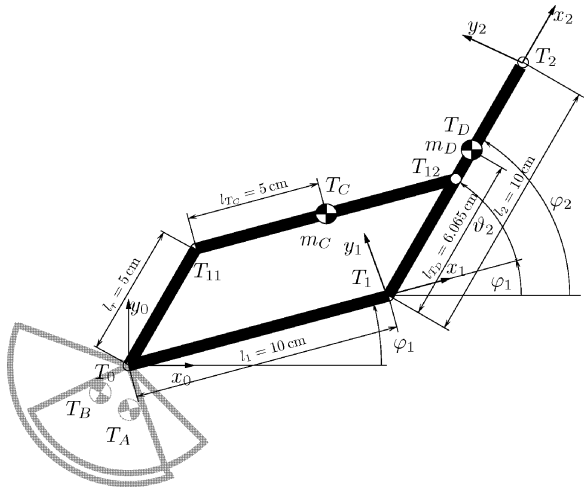

Fig. 4. Planar presentation of the mechanism.

human finger was primarily taken into consideration. The resulting workspace range of the device is depicted in Fig. 2 with a dashed line. Angles φ_1 and φ_2 (see also Fig. 4) change according to the notations in Table III to cover the entire operational space of the device. The constructed mechanism covers the whole range of finger movement, and thus provides force feedback in any finger position.

The arc segments A and B are driven by two independent motors mounted in the base of the manipulator. This enables decoupled control of link angles. Placing both motors on the base, and the use of a tendon-driven transmission system with low transmission ratios, reduces the inertia felt by the user. To achieve a better haptic performance, the masses and moments of inertia (MOI) of the mechanism were reduced. Each motor is equipped with an optical position encoder with a resolution

TABLE III
DEVICE WORKSPACE SEGMENTS

Workspace segment	φ_1	φ_2
$P_1 \rightarrow P_2$	-40°	$50^\circ \rightarrow 105^\circ$
$P_2 \rightarrow P_3$	$-40^\circ \rightarrow 35^\circ$	$105^\circ \rightarrow 180^\circ$
$P_3 \rightarrow P_4$	$35^\circ \rightarrow 70^\circ$	180°
$P_4 \rightarrow P_5$	70°	$180^\circ \rightarrow 70^\circ$
$P_5 \rightarrow P_6$	$70^\circ \rightarrow 50^\circ$	$70^\circ \rightarrow 50^\circ$
$P_6 \rightarrow P_1$	$50^\circ \rightarrow -40^\circ$	50°

of 144 pulses per revolution. The manipulator's top position resolution reading is 0.1 mm or better.

The mechanism is only capable of providing ground-based forces. Therefore, a suitable wooden hand rest with adjustable height was designed. The user's hand is placed in the hand rest and lightly attached with two bands to prevent hand movement.

B. Actuating System

A dc ironless rotor motor combined with a commutation system using precious metals for the brush gear was used in our application. Due to the absence of an iron core in the motor, rotor inertia is very low and there is no cogging, meaning that the rotor can stop at any angle. The rotation speed is not limited by iron losses, but rather depends only on supply voltage and load torque. The stator consists of a cylindrical two-pole permanent magnet that fits inside a steel tube that encloses the magnetic circuit. This construction provides a distinct advantage in numerous applications where a high-performance drive and servo system are required.

The torque transmission between the motor and the segment can be realized in different ways. Most motorized mechanical transmissions are only designed to carry power in the forward direction, from a torque source at the input, to a passive, power absorbing load at the output. However, if the flow of power switches direction, so that an energetic environment at the output drives the input, then power flows in a backward direction. A transmission with a high transmission ratio allows a relatively small motor to multiply its torque by a set ratio, while reducing its speed by the same ratio. Since motors operate most efficiently at high velocities and low torques if compared to the typical velocity and load requirements of robots, virtually every commercial robot joint employs a velocity reducer. It should be noted that while torque and velocity are changed by the value of the transmission ratio, the motor rotor inertia simultaneously multiplies by the square of the transmission ratio. This is also the reason for the low transmission ratio used in this application.

The present mechanism uses a tendon-driven transmission system with low ratio $k_R \approx 20$. The tendon which drives the arc segment is attached to the first end of the arc segment (A and B), then wound around the drive shaft of the motor, and finally attached to the other end of the same arc segment. Tendon drives are generally classified as *closed-loop* and *open-loop tendon drives*. The closed-loop type is used for driving segments of the present parallel mechanism. This transmission system drives a closed-loop tendon in both directions with one motor.

This means that the number of actuators needed is equal to the number of active degrees of freedom of the manipulator. Power transmission relies on the friction generated between the drive shaft and the tendon. In a closed-loop drive, half of the tendon will be under high tension, while the other portion is not loaded. Although torque can be transmitted in both directions, pretensioning is often necessary to prevent slipping. As a side effect, pretensioning can introduce a significant amount of friction, as well as backlash due to the elastic effect of the tendons. To decrease the pretensioning force, the tendon must be wound around the shaft several times.

The low transmission ratio also makes the mechanism backdrivable. Good backdrivability is essential in the design of devices that can sense forces inherently without resorting to destabilizing force-torque sensor strategies. Backdrivability is a measure of how accurately a force or motion applied at the top end is reproduced at the input end. In a mechanical robot-like linkage, good backdrivability means that a person can grasp the tip of the linkage and move it around effortlessly.

III. Kinematics

Fig. 4 represents the coordinate systems used in the direct kinematic and dynamic models. The centers of gravity (COG) of each segment are depicted as T_A, T_B, T_C, and T_D. Fig. 4 also shows a parallel mechanism representation with relevant dimensions. From the kinematic data $(l_1, l_2, r, l_{T_C}, l_{T_D})$ and known values for φ_1 and φ_2, each point position and orientation $(T_1, T_2, T_{11}, T_{12}, T_C, T_D)$ can be computed and further used for calculating linear and angular velocities of the COG in each segment. The position of the manipulator end point $\boldsymbol{p}(\boldsymbol{\varphi})$ is, according to Fig. 4, defined as

$$\boldsymbol{p}(\boldsymbol{\varphi}) = \begin{bmatrix} T_{2x} \\ T_{2y} \\ 0 \end{bmatrix} = \begin{bmatrix} l_1 \cos\varphi_1 + l_2 \cos\varphi_2 \\ l_1 \sin\varphi_1 + l_2 \sin\varphi_2 \\ 0 \end{bmatrix}. \quad (1)$$

A. Inverse Kinematics

Inverse kinematics enables the calculation of angles φ_1 and φ_2 from the known position of finger support coordinates T_{2x} and T_{2y}. Theoretically, there are two possible solutions. Because of the configuration, $\varphi_1 < \varphi_2$, and thus only one inverse kinematic solution is mechanically feasible, as shown in Fig. 5 in bold.

Radius r is calculated first

$$r = \sqrt{T_{2x}^2 + T_{2y}^2}. \quad (2)$$

The maximum radius value is equal to $r_{\max} = l_1 + l_2 = 20$ cm, and minimum $r_{\min} \approx 5$ cm, which is the simple condition for calculating the inverse kinematics.

The next step is calculation of angles $\alpha \in [0, \pi]$, β, and γ, all based on the relations in Fig. 5

$$\alpha = \arccos\left(\frac{{l_1}^2 + {l_2}^2 - r^2}{2 l_1 l_2}\right) \quad (3)$$

$$\beta = \arccos\left(\frac{r^2 + {l_1}^2 - {l_2}^2}{2 l_1 r}\right) \quad (4)$$

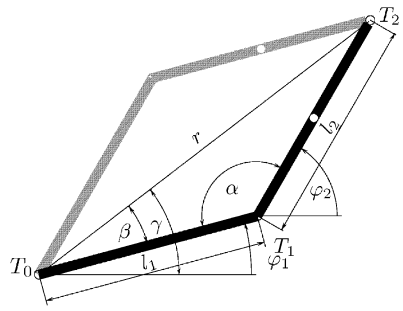

Fig. 5. Variables in the inverse kinematic model.

$$\gamma = \arctan2(T_{2y}, T_{2x}). \quad (5)$$

The values for angles φ_1 and φ_2 can then be computed as

$$\varphi_1 = \gamma - \beta \quad (6)$$

$$\varphi_2 = 180^\circ - \alpha + \varphi_1 = 180^\circ - \alpha - \beta + \gamma. \quad (7)$$

B. Manipulator Analytical Jacobian

To calculate the velocity of the finger support point T_2 from the angular velocities of active joints, a manipulator analytical Jacobian matrix must be defined. The manipulator analytical Jacobian is defined as

$$\mathsf{J}_A(\boldsymbol{\varphi}) = \begin{bmatrix} \frac{\partial T_{2x}}{\partial \varphi_1} & \frac{\partial T_{2x}}{\partial \varphi_2} \\ \frac{\partial T_{2y}}{\partial \varphi_1} & \frac{\partial T_{2y}}{\partial \varphi_2} \end{bmatrix} = \begin{bmatrix} -l_1 \sin\varphi_1 & -l_2 \sin\varphi_2 \\ l_1 \cos\varphi_1 & l_2 \cos\varphi_2 \end{bmatrix}. \quad (8)$$

Finger support velocity depends on joint angular velocities as $\dot{\boldsymbol{p}} = \mathsf{J}_A \dot{\boldsymbol{\varphi}}$, where $\dot{\boldsymbol{p}}$ represents the vector of finger support point velocities and $\dot{\boldsymbol{\varphi}}$ joint angular velocities. Similarly, in static conditions and a rigid-link manipulator, the Jacobian also defines a simple force-torque relationship between the end-effector and the actuators as $\boldsymbol{\tau} = {\mathsf{J}_A}^T \boldsymbol{f}$, where $\boldsymbol{f}$ represents the forces exerted on the end-effector, and $\boldsymbol{\tau}$ represents the torques exerted by the actuators.

C. Force Characteristics Analysis

The traditional force ellipsoid describes all the end-effector forces that a robot can produce, given actuator torques of unit norm $\boldsymbol{\tau}^T \boldsymbol{\tau} = 1$ [16]. For our two-link planar mechanism, the output force is then calculated as $\boldsymbol{f} = {\mathsf{J}_A}^{-T} \boldsymbol{\tau}$. A simple calculation reveals that the force ellipsoid has principal axis vectors $\boldsymbol{v}_i$ with magnitudes $1/\lambda_i$, where $\boldsymbol{v}_i$ and λ_i are the eigenvectors and eigenvalues of $\mathsf{J}_A {\mathsf{J}_A}^T$. The force ellipsoid is perpendicular to the manipulability ellipsoid, indicating that the directions in which the robot can exert the greatest forces are also the directions in which it is least sensitive to changes in the actuator displacements. Fig. 6 shows force ellipsoids at different manipulator positions. Two force scales are depicted, first for the continuous mode, where the maximum current through the

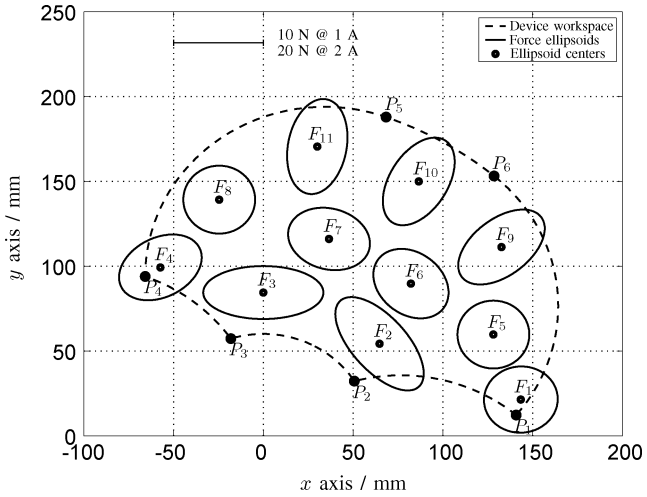

Fig. 6. Force manipulability ellipsoids for the haptic device. Two force scales are depicted: first for the continuous mode, where the maximum current through the motors is limited to 1 A, and second for the short-term mode (5 min.), where the current is limited to 2 A.

motors is limited to 1 A, and second for the short term mode (5 min.), where the current is limited to 2 A. In most postures, the force ellipsoid principal axis vector along the maximum output force is oriented perpendicular to the finger.

1) Maximum Output Force Duration Test: A duration test for the sustained maximum output force was performed, wherein a constant current through the motor was applied. The temperature of the motor was measured using a FLUKE 53 K/J thermometer with typical accuracy within ± 1.1°C. The maximum temperature suggested by international standard [17] is summarized; i.e., applied parts of equipment not intended to supply heat to a patient shall not have a surface temperature exceeding 41 °C. At a current value of 1 A, the temperature did not exceed 41 °C. When a 2 A current was applied, the temperature reached the limit within 5 min. It then takes approximately 40 min. to cool the motor below 25 °C without forced cooling. With normal use, the maximum force is applied for only a few seconds within each exercise, which is not more than 5 min long. Overheating is not present during exercising, and thus does not present difficulties or limitation of use.

IV. Dynamics

Closed form dynamics for the haptic device were derived by using a Lagrangian equation in Cartesian space. For ease of analysis, segments A to D were identified as shown in Fig. 3. Segment rotations and linear velocities were determined first, and later used for kinetic energy calculations. The static friction contribution, which is highly nonlinear, was omitted to simplify analysis.

The following notation is used in the subsequent text: points are denoted with letter T, kinetic energy with K, potential energy V, and losses with P. Gravity is denoted as $g = 9.81$ m/s^2. The kinetic and potential energy, as well as friction losses for individual components, are given as follows.

TABLE IV
Masses and Moments of Inertia of the Segments

	A	B	C	D
mass m/g	129	135	14	24
MOI J/g cm^2	6422	6673	137	207

A. Segments

Table IV specifies masses and MOIs of the segments. MOIs of the segments are defined in the coordinate frames positioned in the COG of each segment, respectively.

Detailed energy components for each segment are defined in Table V. In addition to these known values, there are also unknown parameters, such as f_A and f_B, that characterize viscous friction in ball bearings on each axis, and also all other losses; e.g., losses in the tendon while wrapping around the drive shaft. These two parameters were experimentally estimated through an identification process. Their values are $f_A = f_B \approx 10^{-2}$ kg · m^2/s. Unknown parameter f_C includes the viscous friction in three ball bearings which rotate with the angular velocity $\omega_1 - \omega_2$. The parameter f_C can be neglected due to the large value of f_A and f_B.

B. Motor

Kinetic energy and friction losses of the motor and drive shaft are considered next. The moment of inertia of the rotor is $J_m = 18$ g·cm^2 and of the drive shaft $J_{\text{shaft}} = 2$ g·cm^2. The viscous friction coefficient is $f_m \approx 20 \cdot 10^{-7}$ kg·m^2/s, which was determined by identification and is about 20 times greater than specified by the manufacturer Escap ($f_m = 10^{-7}$ kg·m^2/s). The rotor angular velocity $\omega_{m\,i}$ is determined as $\omega_{m\,i} = k_R\,\omega_i$, where $\omega_i = \frac{d\varphi_i}{d\,t}$ represents the angular velocity, $i = 1, 2$ the index of each of the two motors, and $k_R \approx 20$ is the transmission ratio. Kinetic energy and friction losses for each motor are

$$K_{m\,i} = \frac{1}{2}(J_m + J_{\text{shaft}})\omega_{m\,i}{}^2 \tag{9}$$

$$P_{m\,i} = \frac{1}{2} f_m \omega_{m\,i}{}^2, \qquad i = 1, 2 \tag{10}$$

C. Tendon

Elasticity k_t of the tendon wire stores some potential energy, which moves the driven segment to an unknown neutral position $\varphi_{0\,i}$. From there originate two more unknown parameters for each driven link. Potential energies of the tendon wires are defined as

$$V_{t\,i} = \frac{1}{2} k_{ti}(\varphi_i - \varphi_{0i})^2 \tag{11}$$

where $i = 1, 2$ represents the index for each of two tendons. The cause of the elasticity is the origin pose of the tendon while it was wrapped around the shaft for a prolonged period of time. The tendon acts like a torsion spring which moves toward origin pose. This effect can be avoided by using a very fine plaited tendon.

TABLE V
SEGMENT ENERGIES

	A	B	C	D
kinetic energy K	$\frac{1}{2} J_A \omega_1^2$	$\frac{1}{2} J_B \omega_2^2$	$\frac{1}{2}\left(m_C v_{T_C}^2 + J_C \omega_1^2\right)$	$\frac{1}{2}\left(m_D v_{T_D}^2 + J_D \omega_2^2\right)$
potential energy V	$m_A g T_{Ay}$	$m_B g T_{By}$	$m_C g T_{Cy}$	$m_D g T_{Dy}$
friction losses P	$\frac{1}{2} f_A \omega_1^2$	$\frac{1}{2} f_B \omega_2^2$	$\frac{1}{2} f_C (\omega_1 - \omega_2)^2$	

D. Equations of Motion

With the Lagrangian operator defined as

$$L = K - V \tag{12}$$

where K and V are sums of kinetic and potential energy contributions, respectively, the dynamic equations are derived via

$$\frac{d}{dt}\frac{\partial L}{\partial \dot{\varphi}_i} - \frac{\partial L}{\partial \varphi_i} + \frac{\partial P}{\partial \dot{\varphi}_i} = \tau_i, \qquad i = 1, 2 \tag{13}$$

where P is sum of friction losses

$$\tau_i = k_{I2M} I_{mi}, \qquad i = 1, 2 \tag{14}$$

and τ_i is torque produced by each motor, I_{mi} is the rotor current, and $k_{I2M} = 2$ Ncm/A represents the motor torque constant.

The haptic device dynamic model is written using the matrix notation

$$\mathsf{M}(\varphi)\ddot{\varphi} + \mathsf{C}(\varphi, \dot{\varphi})\dot{\varphi} + \mathsf{F}\dot{\varphi} + \mathsf{K}(\varphi - \varphi_0) + \boldsymbol{G}(\varphi) = \boldsymbol{\tau} \tag{15}$$

where M represents the inertia matrix, C the matrix of Coriolis and centripetal contributions, F the viscous friction matrix, K the elasticity matrix, and $\boldsymbol{G}$ the gravity vector. Further details can be found in [18].

The mechanical design procedure provided estimates for some parameters; e.g., masses, MOIs, dimensions, and transmission ratio. On the other hand, there are other parameters such as the friction of ball bearings or elasticity of the tendon wire, that are not known in advance. The final detailed model includes all relevant contributions and excludes only negligible ones. The mechanical bandwidth of the HIFE system was measured using a variable frequency sine wave signal, and was estimated to be 6 Hz.

V. CONTROL STRUCTURE

The haptic device is controlled by an application running on a personal computer through a custom-designed controller unit. The general connections between the system components are depicted in Fig. 7. The computer is connected to the external controller unit, which includes a real-time clock generator, watchdog timer, power amplifiers for motors, and several safety mechanisms. A personal computer with three data acquisition cards runs the control loop and provides visual feedback of the haptic device.

A. Application

A custom-written application was realized using Borland C++ Builder in the Microsoft Windows operating system (OS). A real-time control strategy within the programming tool in the OS is described in Section V-B. The application enables selection

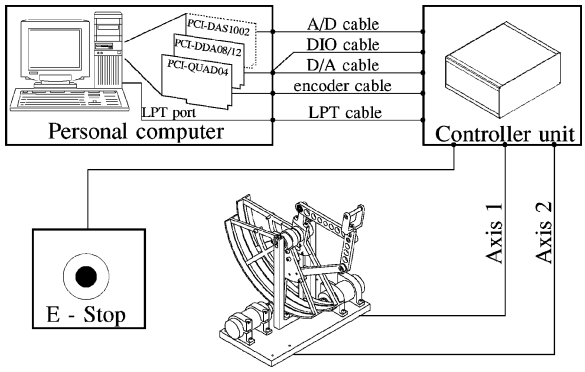

Fig. 7. Connection diagram of the hardware system.

of five different types of robot actions; i.e., finger exercises. The first exercise represents a virtual damper; the second exercise adds a virtual spring, the third is taking the manipulator's end position from a mouse click on the screen, the fourth example represents a record/play option; while in the last choice the reference parameters are MCP and PIP joint angle trajectories. Furthermore, the visual feedback of the device, the contact force, and duration of the exercise are provided to the operator or the person under exercise instantly.

Within the application, an output force is limited in software to the value specified by the user. In all exercise modes, gravity compensation can be switched on or off. Soft start of the exercise is also implemented, which eliminates sudden movements of the haptic device at the beginning of the exercise when the position error is normally high. During the exercise, all the data, including joint angles φ_1 and φ_2, their derivatives, separate contributions of the dynamic model, contact forces, etc., are recorded. The recorded data can be saved to a file for later analysis.

B. Control Strategies

Generally, different control strategies could be used to control the robot in interaction with an environment; i.e., finger [16]. Impedance or direct control schemes enable definition of contact force, or contact force in connection with a position. Due to continuous contact between the finger and the robot, a position control algorithm cannot be used. Even though position following is desired to certain degree, a limited output force is also demanded. If the output force value is too high, the feeling might be uncomfortable, or the finger could even be harmed.

An operational space inverse dynamic controller [16] is used to control the robot (Fig. 8). Inputs are the desired values of the position $\boldsymbol{x}_d$, velocity $\dot{\boldsymbol{x}}_d$, and acceleration $\ddot{\boldsymbol{x}}_d$ of the manipulator end point. Stiffness and viscosity are increasing with increasing

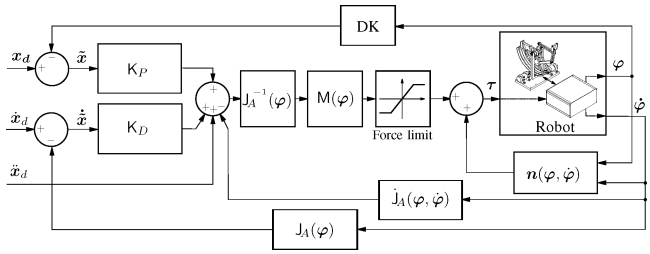

Fig. 8. Operational space inverse dynamics controller scheme.

values of K_P and K_D, respectively. For a compliant motion in connection with a finger, the stiffness value K_P should be set low. Due to this low value, the position error increases when a finger is in contact with the device. The control strategy equation is thus

$$\boldsymbol{\tau} = \mathsf{M}(\boldsymbol{\varphi})\left(\mathsf{J}_A{}^{-1}(\boldsymbol{\varphi})(\ddot{\boldsymbol{x}}_d + \mathsf{K}_P\tilde{\boldsymbol{x}} + \mathsf{K}_D\dot{\tilde{\boldsymbol{x}}} - \dot{\mathsf{J}}_A(\boldsymbol{\varphi},\dot{\boldsymbol{\varphi}})\dot{\boldsymbol{\varphi}})\right) + \boldsymbol{n}(\boldsymbol{\varphi},\dot{\boldsymbol{\varphi}}) \tag{16}$$

where $\boldsymbol{\tau}$ represents the output motor torque reference vector and

$$\boldsymbol{n}(\boldsymbol{\varphi},\dot{\boldsymbol{\varphi}}) = \boldsymbol{G}(\boldsymbol{\varphi}) + \mathsf{C}(\boldsymbol{\varphi},\dot{\boldsymbol{\varphi}})\dot{\boldsymbol{\varphi}} \tag{17}$$

includes gravity and Coriolis contribution compensation (15).

Furthermore, the output force $\boldsymbol{f}$ is calculated as

$$\boldsymbol{f} = \mathsf{J}_A{}^{-T}(\boldsymbol{\varphi})(\boldsymbol{\tau} - \mathsf{M}(\boldsymbol{\varphi})\ddot{\boldsymbol{\varphi}} - \mathsf{C}(\boldsymbol{\varphi},\dot{\boldsymbol{\varphi}})\dot{\boldsymbol{\varphi}} - \mathsf{F}\dot{\boldsymbol{\varphi}} - \boldsymbol{G}(\boldsymbol{\varphi})) \tag{18}$$

where $\mathsf{J}_A{}^{-T}$ represents the inverted transposed Jacobian matrix. Output force $\boldsymbol{f}$ is limited to the value set by the user. In the case when the calculated output force would exceed the limited value, the reference value for the motor current is down-scaled according to the limited force value by using (18).

1) Accuracy of the Trajectory Replay: Accuracy of the trajectory replay was verified for the record/play sequence. First, a trajectory within a whole finger workspace and included nonlinear compensation was recorded. The trajectory was then replayed, first without a finger connected to the device and second, while connected to a finger. Comparison of both tracking errors is presented in Fig. 9.

Several test were performed, and the device consistently followed the recorded trajectory. Without a finger connected to the device, the error is within 2 mm for both axes. The error in the case when a finger is connected is larger than in the previous example, and increases when the finger is moved toward limits of maximum flexion and extension. This is inherent in, and due to, a compliant property of the controller scheme. The error varies slightly among experiments, within reasonable limits. With an increased value of K_P, the error decreases, but the value should stay low to ensure a compliant motion.

2) Accuracy of the Estimated Output Force: The experimental setup consisted of the robotic force-wrist sensor JR3 model 85M31A (JR3 Inc., Woodland, CA) fixed to the base and connected to the top of the HIFE. The output force was set by moving a mouse in four different directions along the base coordinate system, and was limited to 8.1 N within the software. Comparison of the calculated output force and the measured force is presented in Fig. 10. The measured accuracy of the estimated force is better than 10%.

3) Force at Fingertip During Back-Drive: The same experimental setup was used as in the previous experiment. The force sensor was attached to the top of the mechanism and moved around. The trajectory of the movement of the sensor was similar to the finger movement during backdrive. The gravitation of the mechanism was compensated within the software. The average measured back-drive force was 1 N, with a maximum value of 1.5 N.

C. Personal Computer

A personal computer with an AMD Athlon XP 1800+ processor and 512 MB memory was used to run the user application and the control loop. Two data acquisition DAQ cards (Measurement Computing) were connected to the personal computer PCI bus. Communication between data acquisition cards and the software application was written at the PCI card registry level, which was enabled by low-level hardware access drivers [19].

A PCI-DDA08/12 DAQ card with 12-bit analog outputs and digital inputs/outputs was used for analog outputs for torque reference. The digital I/O lines are employed for system status reading. A PCI-QUAD04 is a four-channel quadrature encoder card, and is used for position encoder reading. The system extension includes a PCI-DAS1002 DAQ card with 12-bit analog inputs for motor current monitoring.

D. Controller Unit and Circuits

The controller unit is connected between the personal computer and the haptic device (Fig. 7). Two main custom-designed electronic boards are mounted within the controller unit.

Amplifier electronic boards, one for each axis, convert the torque reference voltage to motor current with a power operational amplifier, L165. Electronics on the amplifier board also transform signals from the motor optical incremental encoder to a quadrature signal. The amplifier board has its own hardware identification bits which must be equal to the motor cable identification number for proper operation. In the case of any unpredictable fault, an emergency button was added, which immediately disconnects the current amplifier power supply voltages. The electronics also enable status checking of the power supplies and the motor connection cable.

The second customized electronic board includes a real-time clock generator for interrupt request (IRQ) triggering, and a watchdog timer for system malfunctions. The board also connects all the lines from the controller unit to the PC and to each amplifier board. All accompanying status signals are also linked to the digital input lines, and can be read by the application.

E. Real-Time Control

Haptic devices must maintain an extremely high update rate (in excess of 500 Hz) if they are to simulate interaction with rapidly-changing force fields [20]. One of the worst cases, and possibly one of the most common in graphics applications, is a collision between the hand-held probe and a simulated hard

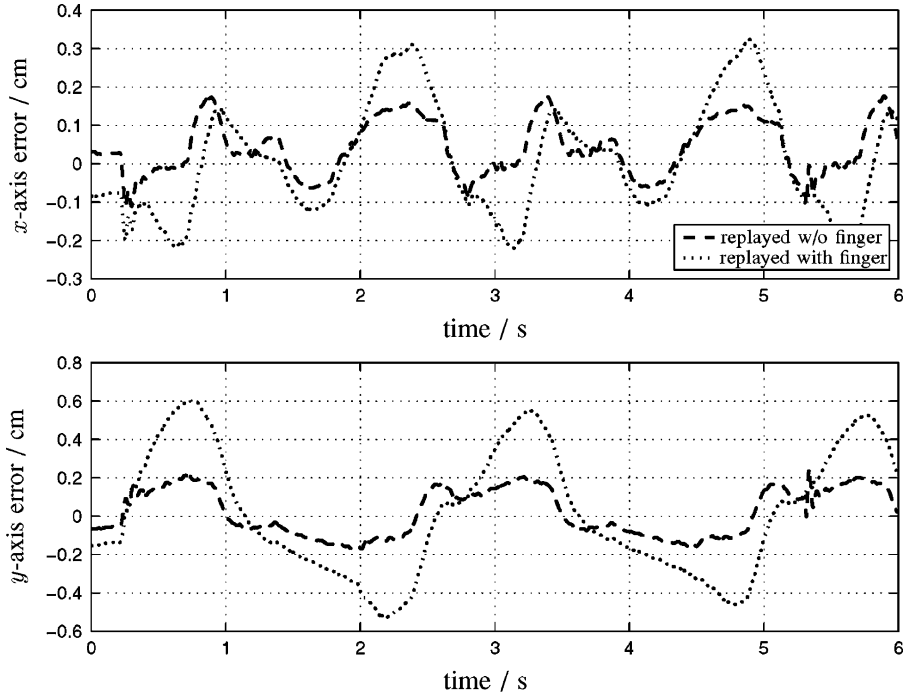

Fig. 9. Accuracy of the followed trajectory with and without a finger connected to the top of the mechanism.

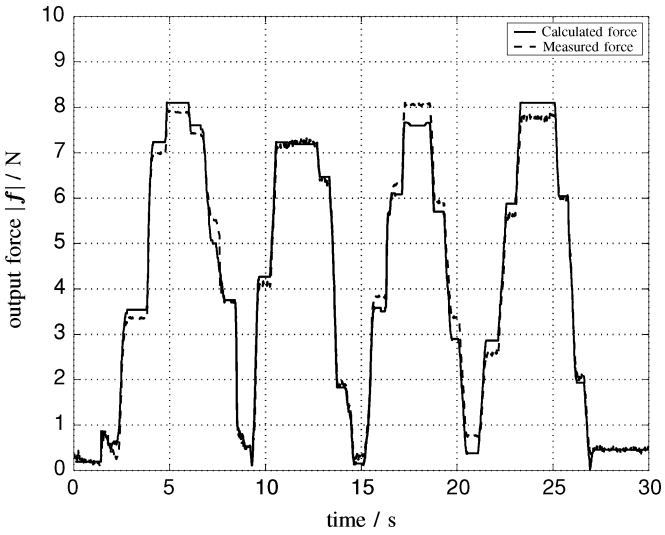

Fig. 10. Calculated output force versus measured force. JR3 force sensor connected to the top of the manipulator was used for force measuring. Accuracy of the estimated output force is within 10%.

surface, such as a wall or table top. As this rate falls below 500 Hz, the user begins to notice high-frequency discontinuities, and any reduction in the update rate reduces the maximum stiffness of stable surfaces.

The planned execution speed of the control loop in this application was at least 1 kHz. Different methods within various development environments and operating systems were tried to fulfill these requirements for timing and low jitter. The timing accuracy of the control loop execution within the RT-Linux operational system is excellent. The main disadvantage of RT-Linux is fairly limited graphical user interface programming tools. However, our goal was the implementation of real-time control within the Microsoft Windows OS, which is very popular among PC users. This is partially due to the variety of available development tools that make programming applications with a sophisticated graphical user interface much easier. The drawback encountered in the Windows environment is strict real-time control, which is in the millisecond-class or even worse. The real-time control system, based on parallel port acknowledge (interrupt) line triggering applied in this solution, is not identical with the RT-Linux hard real-time performance, but is still acceptable. However, it is much easier to implement on any personal computer using the Windows OS. As a third option, the MATLAB-Simulink environment was also tested with "soft" real-time performance while using the time-polling method. In this case, the real-time performance was poor and CPU usage was at 100% all the time.

These were the main arguments for applying the method where the parallel port acknowledge line was used for IRQ triggering. The IRQ number can be specified within the computer BIOS, and is usually set to 7. The interrupt source should be recognized with software code that first unmasks and identifies the interrupt, and then executes the interrupt routine; i.e., control loop. The AT90S2313 AVR RISC series microcontroller from Atmel was used for external real-time clock–RTC generation. The RTC generator and watchdog timer connection scheme is shown in Fig. 11.

The RTC is initialized from the PC by sending the start command through the data lines of the parallel port and triggering the microcontroller IRQ via the strobe line. The initialization sequence enables torque references, starts the RTC timer, and resets all error signals. The RTC then periodically triggers each tick of the real-time control loop by sending the signal through

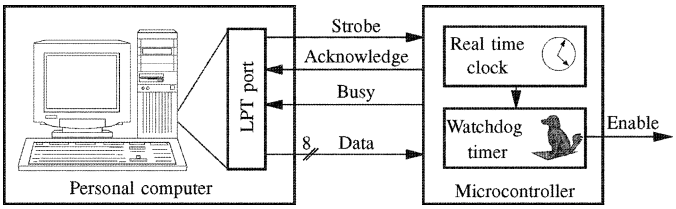

Fig. 11. RTC and watchdog timer connection scheme.

the acknowledge line. The real-time control loop running on the PC responds by sending a dedicated command back to the microcontroller. In this way, the watchdog timer detects proper control loop execution. The operating system overloading, or any other system error related to the RTC, may cause unpredictable behavior of the haptic device, and that calls for independent error checking via an external watchdog timer. If the controller running on the PC does not respond within 2 ms, a first-level error is signalized, while after a 5 ms delay, a second-level error disables torque references and reports the error via the busy line.

The real-time performance of the control loop using the interrupt service in Borland C++ Builder within Windows 2000 OS was compared to RT-Linux and MATLAB-Simulink real-time methods. To obtain an accurate time for evaluation purposes at any given moment within Windows OS, a system function QueryPerformanceCounter() was called. The counter value was divided by its frequency, which was obtained by a system function QueryPerformanceFrequency() call. This makes timer resolution much higher than with any other system timer call value. The sample time for RT-Linux was $1\ \text{ms} \pm 3\ \mu\text{s}$. The real-time performance within the MATLAB-Simulink environment, when the process ran in real-time priority mode, was good. However, as a consequence, the operating system did not respond promptly to user tasks. The time difference between two samples during system overloading increased up to 2.2 ms. With the use of the interrupt service within Borland C++ Builder and Windows OS, the sampling time was $1\ \text{ms} \pm 100\ \mu\text{s}$. The jitter is thirty times that in the RT-Linux OS, but twenty times less than within the MATLAB-Simulink environment, which satisfies our requirements.

F. Safety

One concern present in force-feedback applications is the active safety of the system. Haptic devices, are essentially robot systems, and the user is within the working space of the device. Unlike other display devices; e.g., visual and audio, haptic interfaces might be capable of damaging both themselves and the user when the hardware or software fails.

The haptic device for finger exercise was constructed as a lightweight mechanism, which inherently provides a certain degree of safety. Several safety mechanisms were additionally implemented. Status checking of all functions that could potentially impact the safety of the device is integrated in the control software. The maximal forces are limited within the control system based on the dynamic and kinematic model of the device. The electronic safety mechanisms described previously independently double-check system performance every sample, and disconnect the motor power supply in the case of a failure. In the worst case scenario, the emergency button can be used to power down the device. The system safety could be further improved by requiring the user to take some positive action, such as holding a button for continuous operation, to prevent the device from operating when unattended.

VI. Conclusion

Due to very few haptic interfaces with sufficient output forces and appropriate workspace for fingers, and the high prices of the ones available, a low cost haptic interface with two active degrees of freedom and with a tendon-driven transmission system was developed. The paper presents the development of the interface from the initial concept. The segment lengths of the device were optimized to envelop a finger workspace, and can provide forces up to 10 N, suitable for finger exercise. The kinematic and dynamic model equations with force characteristic analysis, and the control of the haptic device, are presented. The accompanying electronics and real-time control are also described. The application with the haptic interface is running within the Windows operating system, which makes the interface more user friendly. Moreover, the safety of the system was one of the main concerns, and was taken into consideration at every stage of the design. The performance, accuracy, and safety of the device were found to be very good, which makes the device suitable for rehabilitation purposes. For future work, an extended graphical user interface of the application with complete postprocessing and report generation are planned. Clinical validation of the haptic interface for finger exercise in a clinical environment will be performed in the near future.

References

[1] Manitoba, Workplace Injury and Illness, Statistics Report for 2001–2002, Nov. 2003. [Online]. Available: http://www.wcb.mb.ca/publications/archives.html

[2] D. K. Wagener, J. Walstedt, and L. Jenkins, *et al*. Women: Work and health. Vital Health Statistics. 3(31). 1997. [Online]. Available: http://www.cdc.gov/ nchs/data/series/sr_03/sr03_031.pdf

[3] K. E. MacLean and S. S. Snibbe, "An architecture for haptic control of media," in *Proc. 8th Annu. Symp. Haptic Interfaces for Virtual Environment and Teleoperator Systems*, Nashville, TN, Nov. 1999, pp. 1–10.

[4] D. Wollherr and M. Buss, "Cost oriented VR-simulation environment for computer aided control design," in *Proc. 6th IFAC Symp. Cost Oriented Automation*, Berlin, Germany, 2001.

[5] G. Burdea, *Force and Touch Feedback for Virtual Reality*. New York: Wiley, 1996.

[6] T. H. Massie and J. K. Salisbury, "The PHANTOM haptic interface: A device for probing virtual objects," in *Proc. ASME Winter Annu. Meeting, Symp. Haptic Interference for Virtual Environment and Teleoperator Systems*, Chicago, IL, Nov. 1994.

[7] A. Frisoli, F. Simoncini, and M. Bergamasco, "Mechanical design of a haptic interface for the hand," in *Proc. 2002 ASME Int. DETC-27th Biennial Mech. Robot. Conf.*, Montreal, QC, Canada, Sep./Oct. 2002, pp. 2–9.

[8] *PHANToM*, SensAble Technologies. [Online]. Available: http://www.sensable.com/products/ phantom_ghost/phantom.asp

[9] M. Turner, D. Gomez, M. Tremblay, and M. Cutkosky, "Preliminary tests of an arm-grounded haptic feedback device in telemanipulation," in *Proc. ASME IMECE 7th Annu. Symp. Haptic Interfaces*, Anaheim, CA, 1998.

[10] M. Bouzit, G. Burdea, G. Popescu, and R. Boian, "The Rutgers Master II-new design force-feedback glove," *IEEE/ASME Trans. Mechatonics*, vol. 7, no. 2, pp. 256–263, Jun. 2002.

[11] V. Popescu, G. Burdea, M. Bouzit, M. Girone, and V. Hentz, "PC-based telerehabilitation system with force feedback," *Stud. Health Technol. Inform.*, vol. 62, pp. 261–267, 1999.
[12] L. Jones, "Dextrous hands: human, prosthetic and robotic,"*Presence*, vol. 6, no. 1, pp. 29–56, Feb. 1997.
[13] P. Marti, J. M. Fuertes, R. Villa, and G. Fohler, "On real-time control tasks schedulability," presented at the European Control Conf., Porto, Portugal, Sep. 2001, pp. 2227–2232.
[14] B. Wittenmark, J. Nilsson, and M. Törngren, "Timing problems in real-time control systems," presented at the 1995 American Control Conf., Seattle, WA, 1995.
[15] B. Buchholz, T. Armstrong, and S. Goldstein, "Anthropometric data for describing the kinematics of the human hand," *Ergonomics*, vol. 35, no. 3, pp. 261–73, 1992.
[16] L. Sciavicco and B. Siciliano, *Modeling and Control of Robot Manipulators*, 2nd ed. London, U.K.: Springer-Verlag, 2000.
[17] *Medical Electrical Equipment, Part 1: General Requirements for Safety*, International Standard IEC.601-1, 1988.
[18] U. Mali and M. Munih, "Haptic device for finger exercise," in *Proc. 11th Int. Conf. Advanced Robotics-ICAR 2003*, Coimbra, Portugal, Jun./Jul. 2003, pp. 24–30.
[19] "Tvichw32 5.0-The toolkit for directly accessing hardware from Win32 applications," Tech Taiwan, [Online]. Available: http://www.entechtaiwan.com/tvichw32.htm
[20] J. E. Colgate and J. M. Brown, "Factors affecting the z-width of a haptic display," in *Proc. IEEE 1994 Int. Conf. Robotics and Automation*, San Diego, CA, May 1994, pp. 3205–3210.

Uroš Mali received the B.Sc. and M.Sc. degrees in electrical engineering in 2000 and 2003, respectively, from the Faculty of Electrical Engineering, University of Ljubljana, Ljubljana, Slovenia, where he is currently pursuing the Ph.D. degree.

In 1999, he was with the Dynamical Systems and Control Laboratory, The Johns Hopkins University. He is currently an Assistant with the Laboratory of Robotics and Biomedical Engineering, Faculty of Electrical Engineering, University of Ljubljana. His research interests include design, construction, and real-time control of haptic devices and robots for virtual reality supported hand and finger rehabilitation.

Marko Munih (M'88) received the B.Sc., M.Sc., and D.Sc. degrees in electrical engineering from the University of Ljubljana, Ljubljana, Slovenia, in 1986, 1989 and 1993, respectively.

His research interests were focused on functional electrical stimulation of paraplegic lower extremities with surface electrode systems, including measurements, control, biomechanics, and electrical circuits. From 1989, he was Teaching Assistant, and from 1997, Assistant Professor in the Faculty of Electrical Engineering, University of Ljubljana. From 1995 to 1996, he was a Research Assistant with the Implanted Devices Group in the Department of Medical Physics and Bioengineering at University College London and Royal National Orthopaedic Hospital Trust, Stanmore, U.K. His interest focused on robot contact with the environment, and use of haptic interfaces in the field of rehabilitation engineering (projects GENTLE/S, I-Match, Alladin). Currently, he is a Professor and Head of Laboratory of Robotics and Biomedical Engineering at the Faculty of Electrical Engineering, University of Ljubljana.

Dr. Munih received the Zois Award in 2002, given for outstanding scientific contributions by the Slovene Ministry of Science, Education and Sport. He is a member of IFMBE, IFESS, and IFAC.